

# Journal of Environmental Radioactivity

journal homepage: [www.elsevier.com/locate/jenvrad](http://www.elsevier.com/locate/jenvrad)



## Simulating the mesoscale transport of krypton-85

Anne Felsberg<sup>a</sup>, J. Ole Ross<sup>b</sup>, Clemens Schlosser<sup>c</sup>, Gerald Kirchner<sup>a,\*</sup>

<sup>a</sup> Universität Hamburg, ZNF, Hamburg, Germany

<sup>b</sup> Federal Institute for Geosciences and Natural Resources (BGR), Hannover, Germany

<sup>c</sup> Federal Office for Radiation Protection (BfS), Freiburg, Germany

### ARTICLE INFO

#### Keywords:

Atmospheric transport modeling

Uncertainty quantification

Radiokrypton monitoring

HYSPLIT code

### ABSTRACT

Due to its half-life, chemical inertness and low solubility in water, radioactive  $^{85}\text{Kr}$  is a valuable tracer for testing the performance of atmospheric dispersion models in simulating long-range transport of pollutants. This paper evaluates the capability of simulating the dispersion of radiokrypton emitted by a nuclear fuel reprocessing plant in north-west France. Three time periods during which elevated activity concentrations of  $^{85}\text{Kr}$  in ground level air were detected in south-west Germany are chosen. Simulations have been performed using the HYSPLIT code and the European Centre for Median-Range Weather Forecasts (ECMWF) data base. Although their results show a slight trend of underestimating the measured  $^{85}\text{Kr}$  concentrations, there is a significant correlation and moderate scatter between observations and simulations with about 50% of the results being within a factor of two of the measured concentrations. The simulated travel time distributions provided a valuable tool for providing additional insight into the dispersion of the tracer radionuclides and for identifying potential causes of deviations between measured and calculated concentrations.

### 1. Introduction

Atmospheric transport modeling is an indispensable tool for predicting consequences of emissions of hazardous substances. Usually, prime interest is in simulating concentrations in surface air at distances close to the emitter, as potential health impacts may be highest. However, in case of accidents causing high emissions of toxic substances, predicting their mesoscale or even long-range atmospheric transport may be essential for emergency response and impact assessment. A recent example is provided by the Fukushima nuclear accident when atmospheric transport modeling provided information on the source term of radionuclides as well as on their local to regional air concentrations and deposition rates (Katata et al., 2012; Lee et al., 2015; Morino et al., 2011; Stohl et al., 2012; Terada et al., 2012). In support of an assessment of the consequences of the Fukushima nuclear accident conducted by the United Nations Scientific Committee on the Effects of Atomic Radiation (UNSCEAR, 2014), the World Meteorological Organization (WMO) created a task team which provided a multi-model ensemble of simulations of the atmospheric transport and deposition of the emitted radionuclides (Draxler et al., 2015). They concluded that the ensemble mean matched measurements available better than results of any single model (Draxler et al., 2015). Their result is corroborated by the evaluation of multi-model ensemble simulations of the atmospheric dispersion of  $^{133}\text{Xe}$  in western Europe

(Eslinger et al., 2016). This illustrates that there is still a need for tracer data for testing mesoscale atmospheric dispersion simulations.

The radioisotope krypton-85 ( $^{85}\text{Kr}$ ) is an almost ideal atmospheric tracer. It has a half life of 10.76 y, is chemically inert and shows low solubility in water. Its major source is anthropogenic by fission of uranium and plutonium. Both its global inventory and its atmospheric background concentrations are well documented (Ahlswede et al., 2013; Bollhöfer et al., 2014; Inoue et al., 2006). Most of the  $^{85}\text{Kr}$  released into the atmosphere results from civil and military spent fuel reprocessing plants (Ahlswede et al., 2013) from which emission records are not always available, in particular not at a high temporal resolution. As a consequence, this radioisotope has been used only occasionally for validating atmospheric transport models (Connan et al., 2013; Draxler, 1982a,b; Hill et al., 2005; Terada et al., 2013).

In the following, we present results of simulating the atmospheric transport of  $^{85}\text{Kr}$  emitted by the La Hague fuel reprocessing plant over a distance of ca. 740 km to Freiburg, southern Germany (Fig. 1) for three time periods. For these, both emission data and air concentration measurements at the receptor area were available at a high temporal resolution.

\* Corresponding author.

E-mail address: [gerald.kirchner@uni-hamburg.de](mailto:gerald.kirchner@uni-hamburg.de) (G. Kirchner).

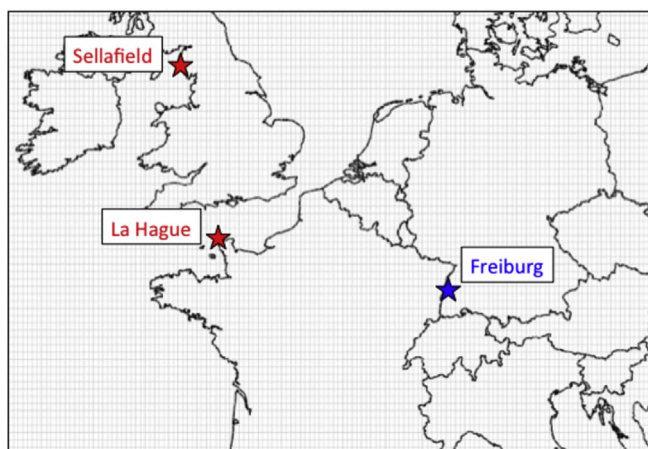


**Fig. 1.** Map of western Europe; given are the  $^{85}\text{Kr}$  emission sources (La Hague, Sellafield), the air sampling location (Freiburg) and the  $0.2^\circ$  concentration grid used with our HYSPLIT simulations.

## 2. Materials and methods

### 2.1. Krypton-85 data

#### 2.1.1. Air concentrations in Freiburg

The German Federal Office for Radiation Protection (BfS) in Freiburg operates a radioactive noble gas laboratory which routinely takes both daily and weekly samples of atmospheric  $^{85}\text{Kr}$ . Its activity is measured by internal gas counting with proportional counters of the chromatographically purified krypton fraction. The volume of krypton in the proportional counter is determined chromatographically by comparison with a calibration gas. As the krypton concentration in the atmosphere is well known ( $1.14 \text{ cm}^3 \text{ m}^{-3}$ ), the activity concentration of  $^{85}\text{Kr}$  in the air samples can be quantified (Schlosser et al., 2017).

Sampling always starts at 7 a.m. UTC (9 a.m. CEST) for the scheduled time period. The sampler is located close to ground on top of a roof in the city centre of Freiburg. The daily samples, however, are analysed only if the corresponding weekly sample shows elevated values compared to the local  $^{85}\text{Kr}$  background of ca.  $1.45 \text{ Bq m}^{-3}$ . During the years 2006–2008 this situation occurred three times: in mid-May 2006, at the end of September 2006 and at the beginning of June 2008. Daily  $^{85}\text{Kr}$  concentrations measured during each of these weeks are shown in Fig. 2.

#### 2.1.2. Emissions from La Hague

The AREVA NC reprocessing facility in La Hague, situated in the north-west of France on the Cotentin peninsula (Fig. 1), operates two units, UP2 and UP3. Together they are the highest emitter of  $^{85}\text{Kr}$  globally (Ahlsweide et al., 2013). Stack releases of this radionuclide are monitored at both units and its mean concentrations per hour in the off-gas are recorded. For our mesoscale transport simulations the emissions of these two adjacent units were treated as a single point source. Hourly emissions during the three time periods covered in this study are shown in Fig. 3.

Recorded hourly concentrations in the off-gas of the two 100 m high stacks of UP2 and UP3 (Connan et al., 2013) were converted to emitted activities of  $^{85}\text{Kr}$  using the methodology developed by Schoetter (2010). It is based on the assumption that the off-gas flow-rate is held constant during plant operation. Using records of the total monthly  $^{85}\text{Kr}$  emissions per unit, mean monthly off-gas flow rates,  $\bar{V} [\text{m}^3 \text{ h}^{-1}]$ , are given as

$$\bar{V}(m) = \frac{E^m}{\sum_{i=1}^{N(m)} C_i} \quad (1)$$

where  $E^m$  [Bq] denotes the activity of  $^{85}\text{Kr}$  emitted in month  $m$ ,  $N(m)$

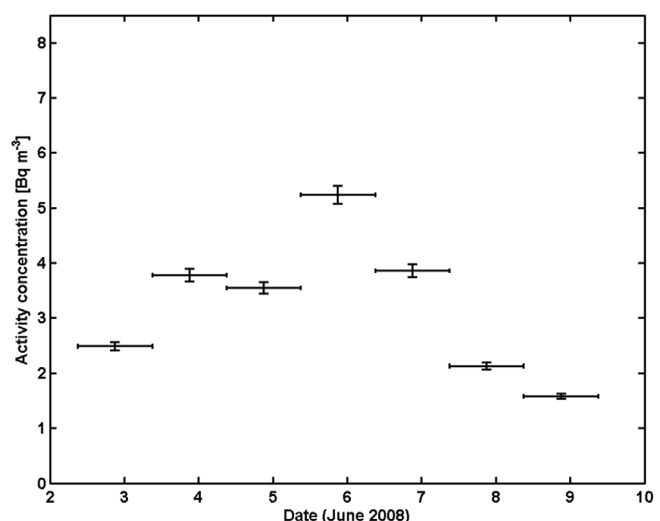
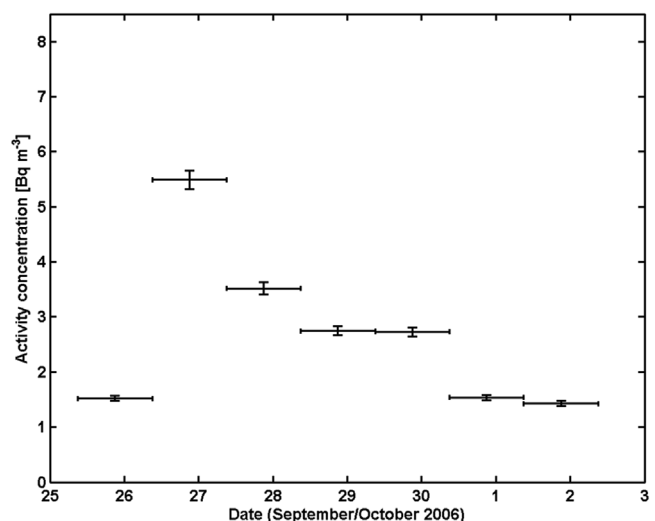
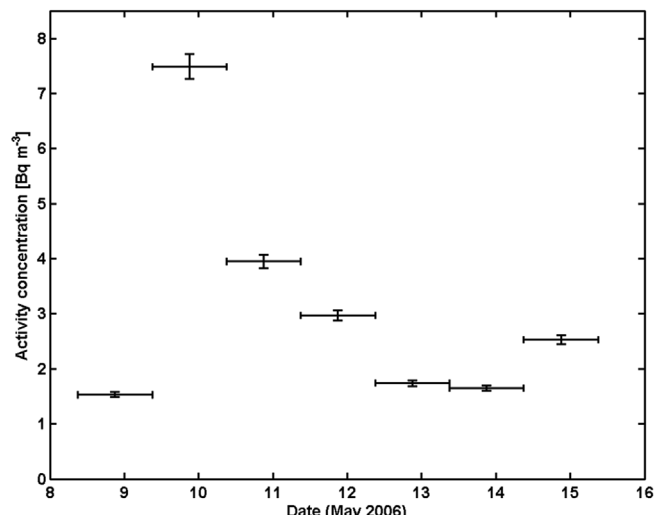


**Fig. 2.** Daily  $^{85}\text{Kr}$  concentrations in air in Freiburg, Germany, during weeks with elevated weekly averages; errorbars denote sampling periods horizontally and analytical uncertainties vertically.

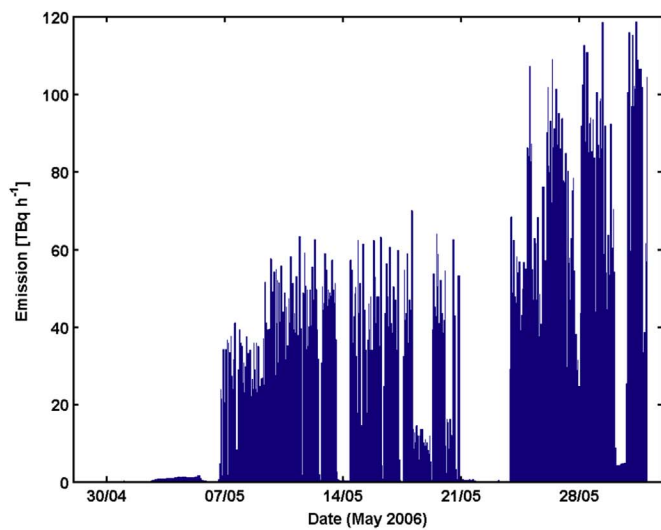


**Fig. 3.** Emissions of  $^{85}\text{Kr}$  from the AREVA NC reprocessing plant in La Hague during the time periods of elevated concentrations in air at Freiburg (Fig. 2).

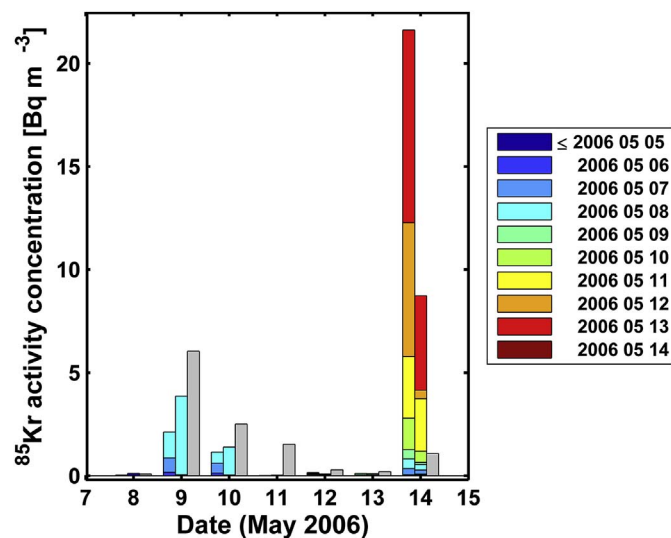


**Fig. 4.** Simulated and measured daily  $^{85}\text{Kr}$  activity concentrations at Freiburg for 8–14 May 2006; grey: measured values above background; coloured: simulated concentrations for resolutions of 0.2° (left) and 0.75° (right) of the meteorological data; colours specify emission dates. (For interpretation of the references to colour in this figure legend, the reader is referred to the web version of this article.)

the number of hours of  $m$ , and  $C_i$  [ $\text{Bq m}^{-3}$ ] the  $^{85}\text{Kr}$  activity concentration in the off-gas at hour  $i$ . Based on records of monthly  $^{85}\text{Kr}$  emissions for three years, Schoetter (2010) found mean values of  $8.52 \times 10^4 \text{ m}^3 \text{ h}^{-1}$  (UP2) and  $1.09 \times 10^5 \text{ m}^3 \text{ h}^{-1}$  (UP3), respectively, with standard deviations  $< 1\%$ . As these small variations confirm the validity of his approach, we adopted these flow rate estimates and converted the activity concentrations,  $C_i$ , recorded per hour  $i$  to the  $^{85}\text{Kr}$  source term,  $I_i^{\text{atm}}$  [ $\text{Bq h}^{-1}$ ], by

$$I_i^{\text{atm}} = \bar{V}^{\text{UP2}} \cdot C_i^{\text{UP2}} + \bar{V}^{\text{UP3}} \cdot C_i^{\text{UP3}}. \quad (2)$$

### 2.1.3. Other emitters

The fuel reprocessing plant in Sellafield, located at the British coast of the Irish Sea (Fig. 1), is the second major emitter of  $^{85}\text{Kr}$  in Europe. However, for this site only monthly emission records were provided by Sellafield Ltd. which for the three time periods studied here are about one order of magnitude below the corresponding emissions from La Hague.

### 2.2. Atmospheric transport model

All simulations have been performed with the Lagrangian model HYSPLIT (Hybrid Single-Particle Langrangian Integrated Trajectory), which has been developed by the U.S. National Oceanic and Atmospheric Administration Air Resources Laboratory (Stein et al., 2015) and is available online. It simulates dispersion of a pollutant either by puffs (with top hat or Gaussian density distribution) or by multiple particle trajectory simulations. For our simulations we chose the latter option. For details of the HYSPLIT methodology and its applications the reader is referred to Stein et al. (2015) and the documents available online.<sup>1</sup>

### 2.3. Simulations

The meteorological data used for our simulations were taken from the European Centre for Medium-Range Weather Forecasts (ECMWF) from two different datasets and converted to the binary HYSPLIT input format. ERA-Interim reanalysis data (Dee et al., 2011) are provided 6-

<sup>1</sup> [http://www.arl.noaa.gov/HYSPLIT\\_pubs.php](http://www.arl.noaa.gov/HYSPLIT_pubs.php) (last accessed 27 April 2017).

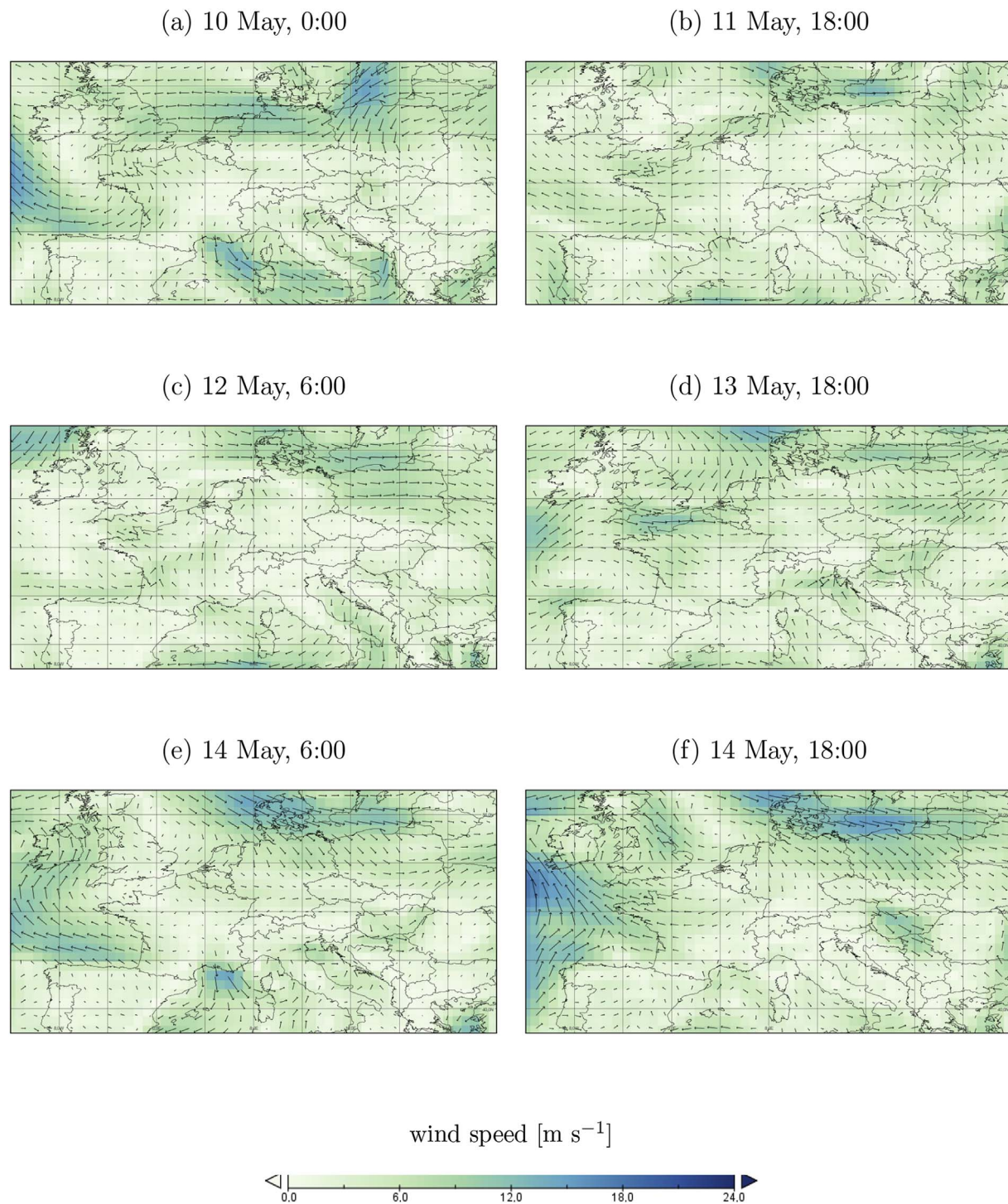
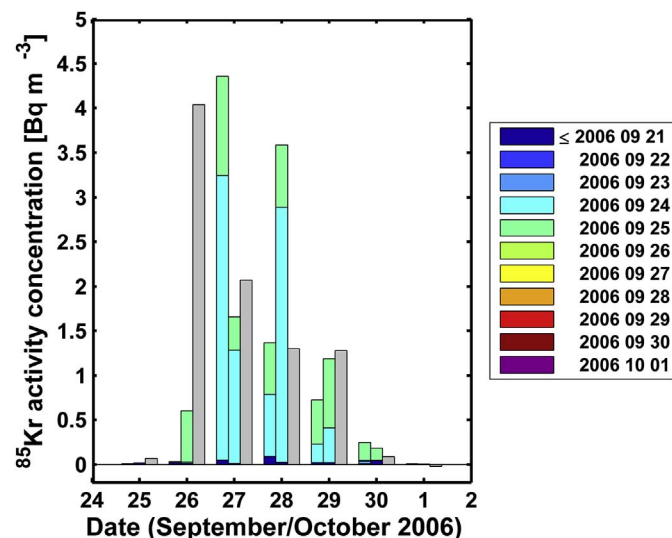


Fig. 5. Evolution of wind speed and direction at 975 hPa (ca. 250 m above ground level) for 10–15 May 2006; data are taken from the ERA-Interim data base.

hourly with 0.75° horizontal resolution on 60 vertical levels. For the simulations with 0.2° horizontal resolution of the meteorological input, operational ECMWF analysis data were retrieved (6-hourly, 91 vertical levels). For both sets of simulations using meteorological data of either 0.75° or 0.2° horizontal resolution, corresponding to approximately 68 km and 18 km, the horizontal resolution of the HYSPLIT concentration grid was set to 0.2°. Although the ECMWF meteorological model reaches up to a pressure level of 0.1 hPa vertically, the transport model was restricted to the troposphere and the model top height in HYSPLIT was set to 10,000 m. The vertical layer over which  $^{85}\text{Kr}$  concentrations were averaged for Freiburg reached from ground level

to 100 m altitude. This is slightly higher than the vertical position of the air sampler several meters above ground but improves particle statistics and representation of local mixing effects compared to restricting the layer to the actual sampler height.

The release point was set to the location of the AREVA NC reprocessing plant in La Hague, France (49.7° N, 1.88° W) at a height of 100 m above ground level, corresponding to the actual height of the UP2 and UP3 stacks. Each simulation included a 24 h emission period with 20,000 particles emitted per hour. The first simulation was performed for a day 2–3 weeks before daily sampling commenced. This was repeated for every day until the last day of the sampling week was



**Fig. 6.** Simulated and measured daily  $^{85}\text{Kr}$  activity concentrations at Freiburg for 25. September - 1. October 2006; grey: measured values above background with error bars denoting their standard deviations; coloured: simulated concentrations for resolutions of  $0.2^\circ$  (left) and  $0.75^\circ$  (right) of the meteorological data; colours specify emission dates. (For interpretation of the references to colour in this figure legend, the reader is referred to the web version of this article.)

reached, resulting in a total of 78 simulations for each grid resolution. The simulations always covered the time period until the last sample was taken in Freiburg. Simulating atmospheric transport using consecutive 24 h emission episodes provides the ability to trace back the emission periods primarily contributing to the measured activity concentrations and to estimate  $^{85}\text{Kr}$  travel time distributions. Model output was generated for every hour. Thus, the timing of the daily sampling periods in Freiburg (7–7 UTC) could be reproduced by summing the hourly concentrations calculated for these at the grid cell of Freiburg ( $48^\circ \text{N}, 7.8^\circ \text{E}$ ).

Due to the lack of time-resolved  $^{85}\text{Kr}$  emission data at the Sellafield site, potential contributions from this source to the concentrations detected at Freiburg could not be taken into account in our simulations. However, the monthly emission records were instrumental in assessing the potential impact of this simplification.

### 3. Results and discussion

In this section, results are presented individually for each of the three simulated time periods and compared to the observed  $^{85}\text{Kr}$  concentrations followed by a combined evaluation. For the sake of clarity, results of the daily sampling performed from 7 to 7 (UTC) of the following day always are assigned to the date sampling started.

#### 3.1. Episode 1: May 8–14, 2006

For this time period, results of our HYSPLIT simulations are shown in Fig. 4 together with the measured  $^{85}\text{Kr}$  activity concentrations above background. The simulations well reproduce the day-to-day variations of the observations. Concentrations predicted by the simulations using a coarser meteorological data grid always better match measurements than those based on a  $0.2^\circ$  grid resolution. For the last day of the sampling interval, however,  $^{85}\text{Kr}$  concentrations are considerably overestimated – by a factor of approx. 7 at  $0.75^\circ$  resolution.

Since this discrepancy appears at the last day of the sampling period, one could hypothesize that air masses with high  $^{85}\text{Kr}$  concentrations could have been present at Freiburg the day after and that even a slight underestimation of transport times could have induced the overestimation. We can rule out such an effect, since the routine weekly

sample taken in the following week showed a concentration of  $1.54 \pm 0.05 \text{ Bq m}^{-3}$  which is not elevated but corresponds to the  $^{85}\text{Kr}$  background.

Alternatively, the  $^{85}\text{Kr}$  concentrations transported to Freiburg could have been overestimated. Since major fractions of krypton predicted to be present in air in Freiburg at May 14 originate from emissions at La Hague of the previous days, we focus our analysis of wind fields in the ERA-Interim data base on May 10–14. Fig. 5 displays 975 hPa wind fields (ca. 250 m above ground), since our HYSPLIT simulations indicate that the vertical  $^{85}\text{Kr}$  concentration maximum centre during transport was well below 500 m above ground level. For the whole time period, 975 hPa and 1000 hPa (ca. 100 m above ground) wind fields closely agreed.

While emissions at the La Hague site were first transported to the south on May 10 (Fig. 5a), wind directions shifted westwards during the day. This direction prevailed over the source-receptor area until the evening of May 11 (Fig. 5b), before gradually turning northward (Fig. 5c). During the afternoon of May 13 westerly winds developed (Fig. 5d). The morning of May 14 experienced an extended calm (Fig. 5e). In the evening wind speed increased, dominantly in the direction south and west over the source-receptor area (Fig. 5f). Thus atmospheric conditions favored transport of  $^{85}\text{Kr}$  emitted at La Hague to Freiburg only during May 13, about 12:00, to May 14, about 6:00. However, after May 13, 13:00 releases dropped by more than two orders of magnitude for 21 h (Fig. 3). This indicates that the 6 h discretization of the ERA-Interim data may be too coarse for adequately taking into account the rapid changes both in wind directions and krypton emissions during May 13. The travel time distributions of the simulated high concentrations on May 14 displayed in Fig. 4 indicate that they originate from  $^{85}\text{Kr}$  emitted between May 10 and May 12. These had been transported to the west and north of La Hague before wind directions reversed towards the receptor area.

Emissions at the Sellafield site were transported in directions opposite to the receptor area with western and northeastern winds until the end of May 12 (Fig. 5a–c). Then, southern winds developed which together with the eastern winds over France created a transport route to Freiburg. This situation prevailed during May 13 (Fig. 5d), but at the beginning of May 14 winds at Sellafield moved to northern and western directions again (Fig. 5e and f). Thus,  $^{85}\text{Kr}$  from Sellafield is unlikely to have contributed to the elevated concentrations measured in Freiburg during May 9–11 (Fig. 4), but this can not be excluded for the May 14 sample.

#### 3.2. Episode 2: September 25 – October 1, 2006

For this time period, the results of our HYSPLIT simulations are shown in Fig. 6. With exception of September 28, predictions using the coarse meteorological data grid ( $0.75^\circ$ ) reproduce the sample-to-sample variations of  $^{85}\text{Kr}$  in surface air at Freiburg somewhat better than those with higher spatial resolution ( $0.2^\circ$ ). For five of the samples, the calculated activity concentrations closely agree with the values measured ( $0.75^\circ$  meteorological data grid), but differ for two samples. According to the travel times given in Fig. 6, the elevated concentrations of  $^{85}\text{Kr}$  present in Freiburg between September 26 and 30 were emitted at La Hague during September 24 and 25. Over these days,  $^{85}\text{Kr}$  emissions by the La Hague plant were high (Fig. 3). Wind fields throughout the episode are shown in Fig. 7 for the 975 hPa level. Again, these closely agree with the 1000 hPa wind fields of the ERA-Interim data base.

As for the preceding days, southerly winds prevailed over France and southwestern Germany on September 24 (Fig. 7a). During the following night, they shifted to westerly winds (Fig. 7b). This situation only changed in the evening of September 26, when an anticyclone developed over western France (Fig. 7c). It moved eastwards during the next day with strong winds from south west starting to dominate in the La Hague area (Fig. 7d); in northeastern France, Switzerland and southern Germany, wind speeds remained low showing varying

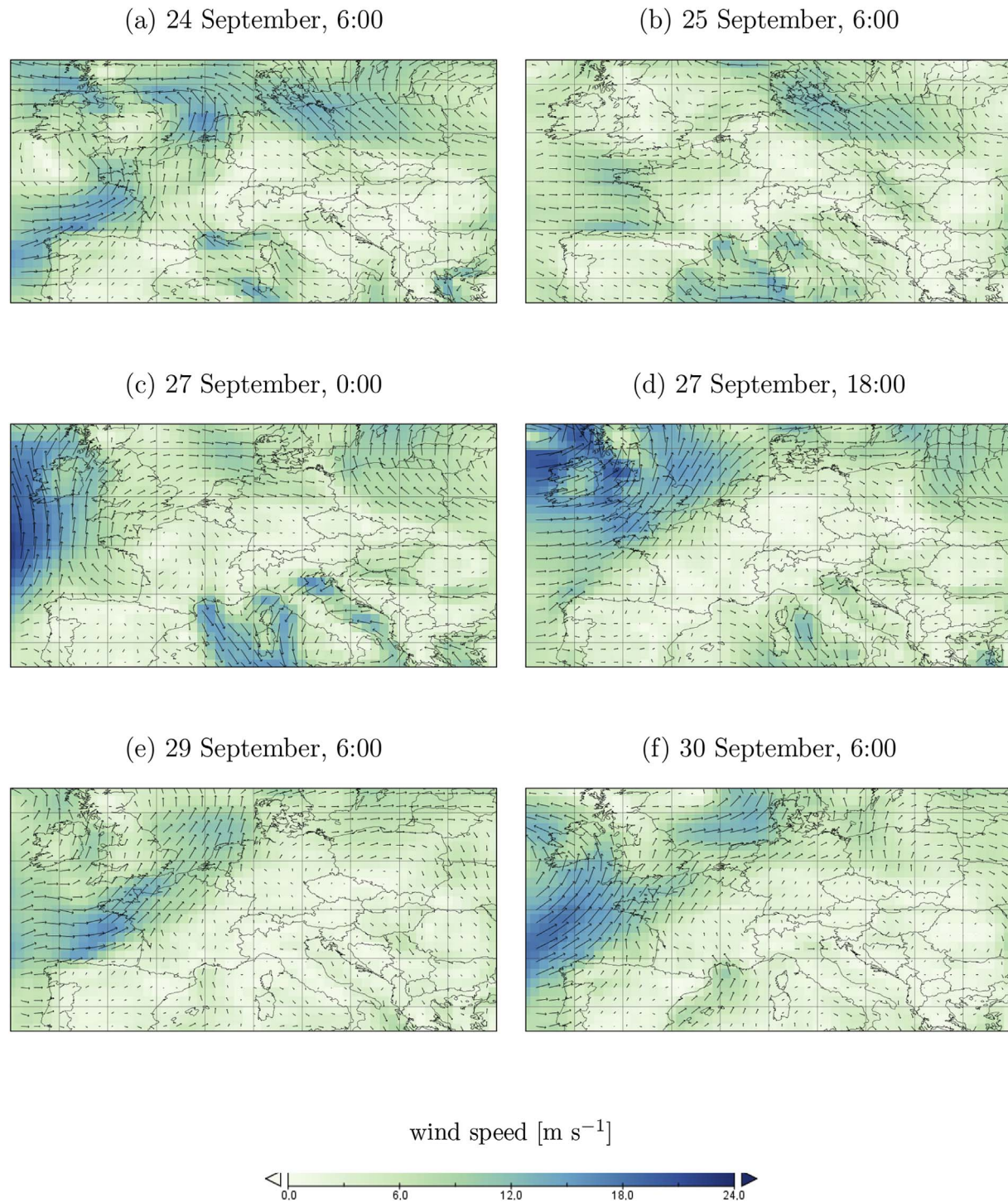


**Fig. 7.** Evolution of wind speed and direction at 975 hPa (ca. 250 m above ground level) for 24–30 September 2006; data are taken from the ERA-Interim data base.

directions. These conditions prevailed (Fig. 7e and f) until the first days of October.

In summary, the meteorological conditions favored direct transport of  $^{85}\text{Kr}$  from La Hague towards Freiburg between the night of September 24 and the evening of September 27, but precluded it before and afterwards. Concentrations in air present at the receptor area on September 27 evening, however, changed only slowly due to the calm wind during the subsequent three days. This is reflected by the elevated concentrations both measured and simulated. Wind speeds were quite low during the direct dispersion phase (Fig. 7b and c) resulting in the considerable transport times shown in Fig. 6, e.g. of  $> 40$  h for a mean

wind speed of  $5 \text{ m s}^{-1}$ .

As our measurements represent 24 h means, small shifts of the simulated travel times caused by the spatial and temporal discretization may result in erroneously assigning an elevated concentration to the preceding or following sample. This effect could explain the deviations between some of the mean 24 h concentrations we simulated and the corresponding measured values. This interpretation is supported by the fact that the differences decrease if we calculate the mean  $^{85}\text{Kr}$  concentrations for the period of 26–29 September giving values of  $2.17 \text{ Bq m}^{-3}$  (measured) and  $1.62/1.76 \text{ Bq m}^{-3}$  (simulated,  $0.2^\circ/0.75^\circ$  spatial resolution of the meteorological data), respectively.

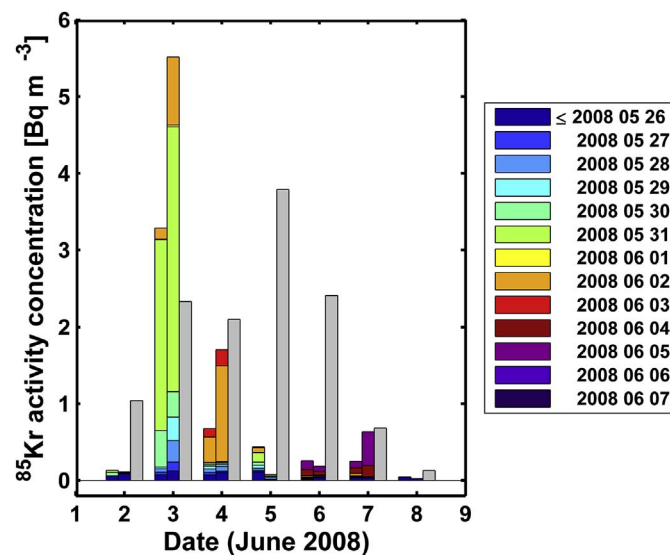


**Fig. 8.** Simulated and measured daily  $^{85}\text{Kr}$  activity concentrations at Freiburg for 1–8 June 2008; grey: measured values above background with error bars denoting their standard deviations; coloured: simulated concentrations for resolutions of  $0.2^\circ$  (left) and  $0.75^\circ$  (right) of the meteorological data; colours specify emission dates. (For interpretation of the references to colour in this figure legend, the reader is referred to the web version of this article.)

Although calculated travel times are considerably larger than for the two other episodes evaluated, model predictions did not deteriorate. This was confirmed by the Mann-Whitney test which showed that differences between simulated and measured  $^{85}\text{Kr}$  concentrations were not significantly higher for this episode than for episodes 1 and 3.

At the Sellafield site, western winds dominated during the first days at the beginning of our period of interest (Fig. 7a). During the evening of September 25, these turned to east in direction of Denmark and northern Germany. In the following night, northern winds developed which prevailed until the first days of October (Fig. 7c–f). Thus, transport of Sellafield  $^{85}\text{Kr}$  to Freiburg could have affected our measured concentrations for some time period during September 27, if plant emissions were high during these hours.

### 3.3. Episode 3: June 2–8, 2008

For the third period considered in our study, day-to-day variations of simulated  $^{85}\text{Kr}$  concentrations for both meteoreological data grid resolutions fairly well reproduce those observed on four days of the sampling week, but not on the 2nd, 5th and 6th of June (Fig. 8). For this episode, calculated source-receptor travel times of 2–3 days dominate. Throughout this episode, emissions of  $^{85}\text{Kr}$  showed considerable fluctuations, but only dropped to low values during the morning of June 3 (Fig. 3). The ERA-Interim wind fields during the relevant time period are displayed in Fig. 9 for the 975 hPa level. As previously, the 1000 hPa wind fields show no major differences.

During May 31, winds from north to northeast prevailed over France (Fig. 9a) precluding any direct transport from La Hague to Freiburg. On June 1, a low pressure system developed over the eastern Biscaya causing air masses to circulate with direction southwards over western France, but contrarily in its east (Fig. 9b). This depression slowly moved northward towards La Hague covering Freiburg on June 2 (Fig. 9c). With the cyclone approaching the North Sea, its circulation created a direct source-receptor pathway which was present until the evening of June 4. Then winds from the Atlantic and from East Europe mixed over France (Fig. 9d). On 6th June, winds over the source-receptor area turned eastwards again (Fig. 9e). About 30 h later winds started to come from north (Fig. 9f), thus precluding direct transport of  $^{85}\text{Kr}$  from La Hague to Freiburg, and shifted westwards on June 9.

Taking into account travel times, the wind field data explain why radiokrypton concentrations in Freiburg were low before June 2 and after June 7. Starting from June 1, radiokrypton emitted at La Hague was first transported towards the Biscaya, before the low pressure system present over France carried it to Freiburg via southern France during the next days. This caused the elevated concentrations observed during June 2–4. Again, even small shifts of simulated travel times caused by the discretization may explain the differences between measured and calculated mean 24 h concentrations. For the two following days, however, our simulations consistently underestimate measured  $^{85}\text{Kr}$  (Fig. 8). Since atmospheric conditions over Europe were dominated by winds from the southwest and east meeting over the southern North Sea (Fig. 9d), our simulations apparently did not correctly reproduce the mixing of air masses contaminated by the emissions from La Hague with those originating from central and eastern Europe. The elevated  $^{85}\text{Kr}$  concentration observed at June 7 is caused by winds from the northwest present over France during this and the previous day. Wind speeds were rather high resulting in short  $^{85}\text{Kr}$  travel times within the simulations.

Krypton releases at Sellafield closely followed the dispersion patterns discussed above for the La Hague emissions during the whole period of interest (Fig. 9). Due to the lack of time-resolved emission data for Sellafield  $^{85}\text{Kr}$ , their contribution to the activity concentrations reaching the receptor area cannot be quantified. As total emissions in June 2008 were about one order of magnitude lower than those from La Hague, it is reasonable to assume that this ratio will similarly apply for the elevated concentrations measured at Freiburg.

### 3.4. Performance measures

Statistical procedures have been shown to provide valuable measures for evaluating the performance of atmospheric dispersion modeling tools (Boybeyi et al., 2001; Chang and Hanna, 2004; Draxler et al., 2015; De Meutter et al., 2016; Hanna et al., 1993; Hegarty et al., 2013; Mosca et al., 1998; Stohl et al., 1998). Since each of them shows some limitation, the use of several statistical indices is recommended (Chang and Hanna, 2004). In our analysis various commonly used statistical measures were selected: the fractional bias (FB), the fraction of predictions within a factor of 2 of the measurements (FAC2), the normalized mean squared error (NMSE), the Pearson linear correlation coefficient ( $r_p$ ) and the Spearman rank correlation coefficient ( $R_s$ ).

Table 1 summarizes the results. Since our simulations show exceptionally high concentrations at Freiburg on May 14, 2006, additional statistical analyses have been performed excluding these. For the  $0.75^\circ$  meteorological data grid, there is a small negative fractional bias (FB) of our simulations which becomes more distinct if the single large overestimation of May 14, 2006 is excluded. It then corresponds to a mean underestimation of  $0.55 \text{ Bq m}^{-3}$ ; nonetheless the fraction of predictions which are within a factor of 2 of the measurements (FAC2) approaches 50%. As expected, a major part of the scattering (NMSE) is caused by the single overprediction for May 14, 2006. Our analyses impressively illustrate both the sensitivity of the Pearson correlation coefficient  $r_p$  to potential outliers (Chang and Hanna, 2004) and the robustness of the Spearman rank correlation coefficient  $R_s$ . Moreover, the high values of  $R_s$  indicate a significant concordance of our simulations with the observed  $^{85}\text{Kr}$  concentrations.

Chang and Hanna (2004) assume that models providing “good” simulations of concentration variations in space should show values of about  $\pm 0.3$  (FB), 1.5 (NMSE) and 0.5 (FAC2) or better. For the best set of predictions, comparable values are given in Table 1 for the concentration dynamics with time simulated here. Our results are also similar to the statistical evaluations of simulations reported recently by Eslinger et al. (2016) and De Meutter et al. (2016). They use various code and wind field data, but modeled the dispersion of another radioactive noble gas isotope ( $^{133}\text{Xe}$ ) in the same European area as we did from its major emitter in Belgium to the Schauinsland mountain

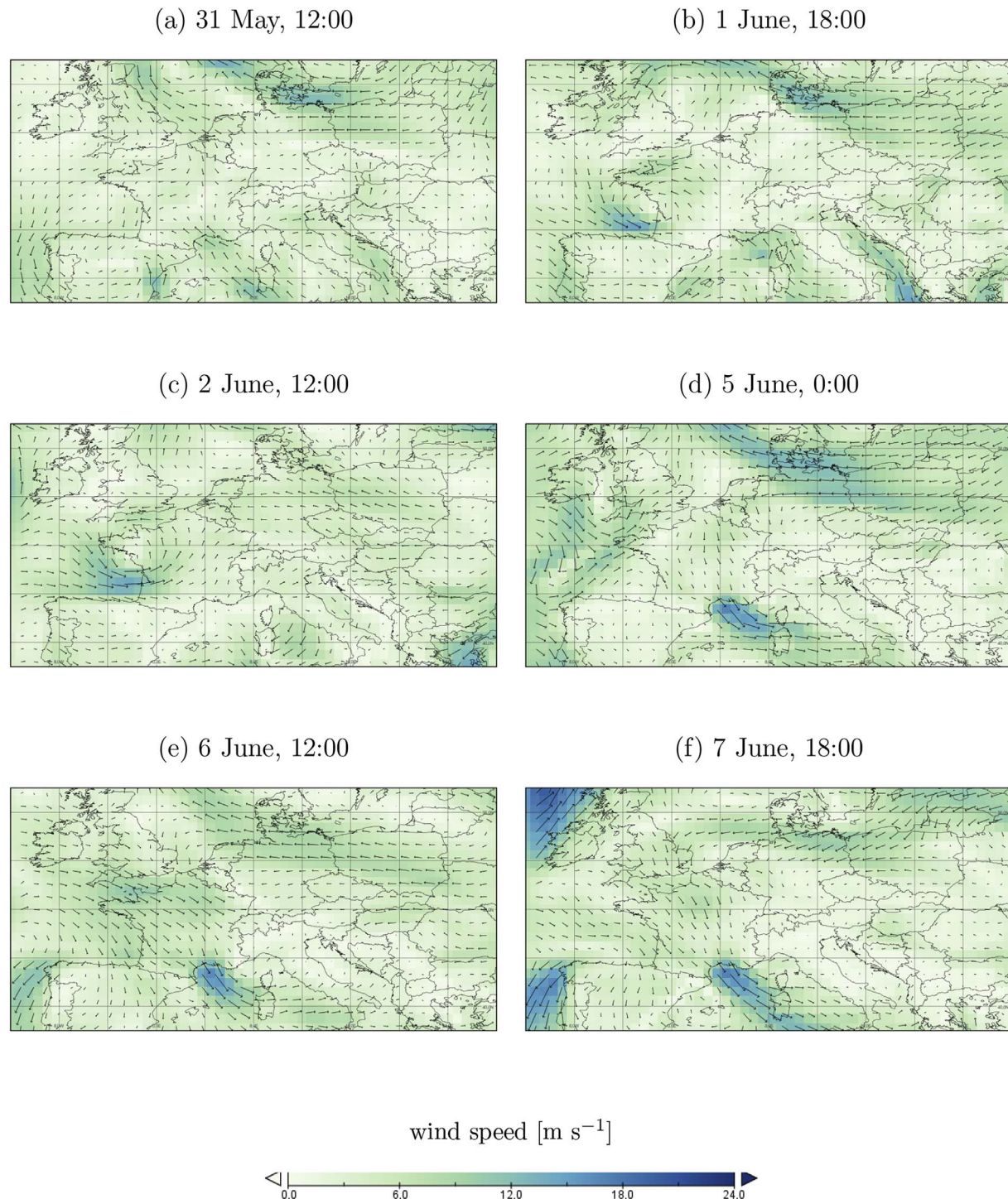


**Fig. 9.** Evolution of wind speed and direction at 975 hPa (ca. 250 m above ground level) for 31. May - 8. June 2008; data are taken from the ERA-Interim data base.

**Table 1**

Values of the statistical measures for the  $^{85}\text{Kr}$  dispersion simulations; grid data denote the resolution of the meteorological data used for the simulations.

Data set	FB	FAC2	NMSE	$r_p^{\text{a}}$	$R_s^{\text{a}}$
0.75°	all data	-0.10	0.43	2.43	0.27
	w/o May 14, 2006	-0.41	0.49	1.65	0.48* 0.60**
0.2°	all data	0.11	0.29	8.28	0.03
	w/o May 14, 2006	-0.70	0.37	2.48	0.40 0.56**

<sup>a</sup>: \*: 0.05 ≥ p > 0.01, \*\*: 0.01 ≥ p > 0.001.

close to Freiburg where activity concentrations were measured.

The statistical analyses of Table 1 confirm that the simulations using a 0.2° resolution of the meteorological data overall gave less satisfactory results, although they improve the spatial resolution of the complex terrain present in major parts of our simulation area (e.g. the Vosges and the Black Forest enclosing the Upper Rhine Valley where Freiburg is located). It could be suspected that the 6 h temporal resolution of the 0.2° ECMWF analysis data was too low for accounting for fast synoptic changes and local orographic effects. However, in two recent atmospheric transport model intercomparison studies experiments performed in the framework of CTBT radioxenon monitoring

(Eslinger et al., 2016; Maurer et al., 2017) the contributions with 6 h temporal resolution of meteorological data did not perform significantly worse. Both studies concluded that a higher spatial resolution of the meteorological fields did not significantly improve the concentration estimates which compares well with the results presented here.

#### 4. Conclusions

We have evaluated the capability of the Lagrangian particle dispersion code HYSPLIT for simulating the transport of the inert noble gas isotope  $^{85}\text{Kr}$  over Europe for three time periods during which elevated concentrations had been observed at 740 km distance from the emitter. Meteorological data have been taken from the European Centre for Median-Range Weather Forecasts (ECMWF) data base. For each episode, a series of consecutive simulations was performed for calculating source-receptor travel time distributions. These turned out to provide considerable additional insight into the dispersion patterns of the radiokrypton detected in Freiburg.

Overall the simulations showed a mean negative bias with about 50% of the results being within a factor of two of the measured concentrations. The scatter was reasonable and may be partly caused by the sampling scheme of taking 24 h samples. Simulated  $^{85}\text{Kr}$  concentrations showed a significant correlation with measured concentrations.

In summary, our study underlines the attractiveness of  $^{85}\text{Kr}$  as a convenient tracer for assessing our capabilities of simulating the long-range transport and dispersion of trace substances in the atmosphere. At present its major limitation may be the restricted availability of emission data with high time resolution.

#### Acknowledgements

We are obliged to Serge Le Bar, AREVA, for providing data of the hourly  $^{85}\text{Kr}$  activity concentrations in off-gas of UP2 and UP3, La Hague, and the colleagues at Sellafield Ltd. for providing monthly emission data. We would like to thank Roland Draxler, NOAA, for his encouragement for pursuing the simulations presented here. We gratefully acknowledge the NOAA Air Resources Laboratory (ARL) for the provision of the HYSPLIT model and the ECMWF for delivering the meteorological data.

This research did not receive any specific grant from funding agencies in the public, commercial or not-for-profit sectors.

#### References

- Ahlswede, J., Hebel, S., Ross, J.O., Schoetter, R., Kalinowski, M.B., 2013. Update and improvement of the global krypton-85 emission inventory. *J. Environ. Radioact.* 115, 34–82. <https://doi.org/10.1016/j.jenvrad.2012.07.006>.
- Bollhöfer, A., Schlosser, C., Ross, J.O., Sartorius, H., Schmid, S., 2014. Variability of atmospheric krypton-85 activity concentrations observed close to the ITCZ in the southern hemisphere. *J. Environ. Radioact.* 127, 111–118. <https://doi.org/10.1016/j.jenvrad.2013.10.003>.
- Boybeyi, Z., Ahmad, N.N., Bacon, D.P., Dunn, T.J., Hall, M.S., Lee, P.C.S., Sarma, R.A., Wait, T.R., 2001. Evaluation of the operational multiscale environment model with grid adaptivity against the European tracer experiment. *J. Appl. Meteorol.* 40, 1541–1558.
- Chang, J.C., Hanna, S.R., 2004. Air quality model performance evaluation. *Meteorol. Atmos. Phys.* 87, 167–196. <https://doi.org/10.1007/s00703-003-0070-7>.
- Connan, O., Smith, K., Organo, C., Solier, L., Maro, D., Hébert, D., 2013. Comparison of RIMPUFF, HYSPLIT, ADMS atmospheric dispersion model outputs, using emergency response procedures, with  $^{85}\text{Kr}$  measurements made in the vicinity of a nuclear fuel reprocessing plant. *J. Environ. Radioact.* 124, 266–277. <https://doi.org/10.1016/j.jenvrad.2013.06.004>.
- Dee, D.P., Uppala, S.M., Simmons, A.J., Berrisford, P., Poli, P., Kobayashi, S., Andrae, U., Balmaseda, M.A., Balsamo, G., Bauer, P., Bechtold, P., Beljaars, A.C.M., van de Berg, L., Bidlot, J., Bormann, N., Delsol, C., Dragani, R., Fuentes, M., Geer, A.J., Haimberger, L., Healy, S.B., Hersbach, H., Hölm, E.V., Isaksen, L., Källberg, P., Köhler, M., Matricardi, M., McNally, A.P., Monge-Sanz, B.M., Morcrette, J.-J., Park, B.-K., Peubey, C., de Rosnay, P., Tavolato, C., Thépaut, J.-N., Vitart, F., 2011. The ERA-Interim reanalysis: configuration and performance of the data assimilation system. *Q. J. R. Meteorol. Soc.* 137, 553–597. <https://doi.org/10.1002/qj.828>.
- De Meutter, P., Camps, J., Delcloo, A., Deconninck, B., Termonia, P., 2016. On the capability to model the background and its uncertainty of CTBT-relevant radionuclides in Europe by using ensemble dispersion modeling. *J. Environ. Radioact.* 164, 280–290. <https://doi.org/10.1016/j.jenvrad.2016.07.033>.
- Draxler, R.R., 1982a. Testing a mesoscale model with the Savannah River Plant krypton-85 air concentration data. *Atmos. Environ.* 16, 1261–1264.
- Draxler, R.R., 1982b. Measuring and modeling the transport and dispersion of krypton-85 1500 km from a point source. *Atmos. Environ.* 16, 2763–2776.
- Draxler, R.R., Arnold, D., Chino, M., Galmarini, S., Hort, M., Jones, A., Leadbetter, S., Malo, A., Maurer, C., Rolph, G., Saito, K., Servranckx, R., Shimbori, R., Solazzo, E., Wotawa, G., 2015. World Meteorological Organizations model simulations of the radionuclide dispersion and deposition from the Fukushima Daiichi nuclear power plant accident. *J. Environ. Radioact.* 139, 172–184. <https://doi.org/10.1016/j.jenvrad.2013.09.014>.
- Eslinger, P.W., Bowyer, T.W., Achim, P., Chai, T., Deconninck, B., Freeman, K., Generoso, S., Hayes, P., Heidmann, V., Hoffman, I., Kijima, Y., Krysta, M., Malo, A., Maurer, C., Ngan, F., Robins, P., Ross, J.O., Saunier, O., Schlosser, C., Schöppner, M., Schrom, B.T., Seibert, P., Stein, A.F., Ungar, K., Yi, J., 2016. International challenge to predict the impact of radionuclide releases from medical isotope production on a comprehensive nuclear test ban treaty sampling station. *J. Environ. Radioact.* 157, 41–51. <https://doi.org/10.1016/j.jenvrad.2016.03.001>.
- Hanna, S.R., Chang, J.C., Strimaitis, D.G., 1993. Hazardous gas model evaluation with field observations. *Atmos. Environ.* 27A, 2265–2285.
- Hegarty, J., Draxler, R.R., Stein, A.F., Brioude, J., Mountain, M., Eluszkiewicz, J., Nehrkorn, T., Ngan, F., Andrews, A., 2013. Evaluation of Lagrangian particle dispersion models with measurements from controlled tracer releases. *J. Appl. Meteorol. Climatol.* 52, 2623–2637. <https://doi.org/10.1175/JAMC-D-13-0125.1>.
- Hill, R., Taylor, J., Lowles, I., Emmerson, K., Parker, T., 2005. A new model validation database for evaluating AERMOD, NPPR R91 and ADMS using krypton-85 data from BNFL Sellafield. *Int. J. Environ. Pollut.* 24, 75–87. (2005). <https://doi.org/10.1504/IJEP.2005.007386>.
- Inoue, H.Y., Matsueda, H., Igarashi, Y., Sawa, Y., Wada, A., Nemoto, K., Sartorius, H., Schlosser, C., 2006. Seasonal and long-term variations in atmospheric  $\text{CO}_2$  and  $^{85}\text{Kr}$  in Tsukuba, Central Japan. *J. Meteorol. Soc. Jpn.* 84, 959–968.
- Katata, G., Ota, M., Terada, H., Chino, M., Nagai, H., 2012. Atmospheric discharge and deposition of radionuclides during the Fukushima Dai-ichi Nuclear Power Plant accident. Part I: source term estimation and local-scale atmospheric dispersion in early phase of the accident. *J. Environ. Radioact.* 109, 103–113. <https://doi.org/10.1016/j.jenvrad.2012.02.006>.
- Lee, K.-H., Kim, K.-H., Lee, J.-H., Jun, J.-Y., Kim, C.-H., 2015. Modeling of long range transport pathways for radionuclides to Korea during the Fukushima Dai-ichi nuclear accident and their association with meteorological circulations. *J. Environ. Radioact.* 148, 80–91. <https://doi.org/10.1016/j.jenvrad.2015.06.007>.
- Maurer, C., Kalinowski, M., Kusmierszky-Michulec, B., Bowyer, T., 2017. 2nd ATM challenge 2016. In: CTBT Science and Technology Conference, Vienna, 26–30 June 2017.
- Morino, Y., Ohara, T., Nishizawa, M., 2011. Atmospheric behavior, deposition, and budget of radioactive materials from the Fukushima Daiichi nuclear power plant in March 2011. *Geophys. Res. Lett.* 38 L00G11. <https://dx.doi.org/10.1029/2011GL048689>.
- Mosca, S., Graziani, G., Klug, W., Bellasio, R., Bianconi, R., 1998. A statistical methodology for the evaluation of long-range dispersion models: an application to the ETEX exercise. *Atmos. Environ.* 32, 4307–4324. [https://doi.org/10.1016/S1352-2310\(98\)00179-4](https://doi.org/10.1016/S1352-2310(98)00179-4).
- Schlosser, C., Bollhöfer, A., Schmid, S., Krais, R., Bieringer, J., Konrad, M., 2017. Analysis of radionuclides and Krypton-85 at the BfS noble gas laboratory. *Appl. Radiat. Isot.* 126, 16–19 (2017).
- Schoetter, R., 2010. Noble Gas Treatment and Emission Characteristics of Point Sources with Relevance to Undeclared Nuclear Activities. Diploma Thesis. Dept. of Physics, University of Hamburg.
- Stein, A.F., Draxler, R.R., Rolph, G.D., Stunder, B.J.B., Cohen, M.D., Ngan, F., 2015. NOAA's HYSPLIT atmospheric transport and dispersion modeling system. *B. Am. Meteorol. Soc.* 96, 2059–2077.
- Stohl, A., Hittenberger, M., Wotawa, G., 1998. Validation of the Lagrangian particle dispersion model FLEXPART against large-scale tracer experiment data. *Atmos. Environ.* 32, 4245–4264. [https://doi.org/10.1016/S1352-2310\(98\)00184-8](https://doi.org/10.1016/S1352-2310(98)00184-8).
- Stohl, A., Seibert, P., Wotawa, G., Arnold, D., Burkhardt, J.F., Eckhardt, S., Tapia, C., Vargas, A., Yasunari, T.J., 2012. Xenon-133 and caesium-137 releases into the atmosphere from the Fukushima Dai-ichi nuclear power plant: determination of the source term, atmospheric dispersion, and deposition. *Atmos. Chem. Phys.* 12, 2313–2343. <https://doi.org/10.5194/acp-12-2313-2012>.
- Terada, H., Katata, G., Chino, M., Nagai, H., 2012. Atmospheric discharge and deposition of radionuclides during the Fukushima Dai-ichi nuclear power plant accident. Part II: verification of the source term and analysis of regional-scale atmospheric dispersion. *J. Environ. Radioact.* 112, 141–154. <https://doi.org/10.1016/j.jenvrad.2012.05.023>.
- Terada, H., Nagai, H., Yamazawa, H., 2013. Validation of a Lagrangian atmospheric dispersion model against middle-range scale measurements of  $^{85}\text{Kr}$  concentration in Japan. *J. Nucl. Sci. Technol.* 50, 1198–1212. <https://doi.org/10.1080/00223131.2013.840545>.
- UNSCEAR: United Nations Scientific Committee on the Effects of Atomic Radiation, 2014. Levels and Effects of Radiation Exposure Due to the Nuclear Accident after the 2011 Great East-Japan Earthquake and Tsunami. UNSCEAR 2013 Report, Annex A. United Nations, New York.